Nanoscale

PAPER

View Article Online
View Journal

Cite this: DOI: 10.1039/c3nr05944h

Using ruthenium polypyridyl functionalized ZnO mesocrystals and gold nanoparticle dotted graphene composite for biological recognition and electrochemiluminescence biosensing

Suli Liu,† Jinxing Zhang,† Wenwen Tu, Jianchun Bao and Zhihui Dai*

Received 8th November 2013
Accepted 3rd December 2013

DOI: 10.1039/c3nr05944h

www.rsc.org/nanoscale

Using ruthenium polypyridyl functionalized ZnO mesocrystals as bionanolabels, a universal biological recognition and biosensing platform based on gold nanoparticle (AuNP) dotted reduced graphene oxide (rGO) composite was developed. AuNP–rGO accelerated electron transfer between the detection probe and the electrode, and increased the surface area of the working electrode to load greater amounts of the capture antibodies. The large surface area of ZnO mesocrystals was beneficial for loading a high content ruthenium polypyridyl complex, leading to an enhanced electrochemiluminescence signal. Using α-fetoprotein (AFP) as a model, a simple and sensitive sandwich-type electrochemiluminescence biosensor with tripropylamine (TPrA) as a coreactant for detection of AFP was constructed. The designed biosensor provided a good linear range from 0.04 to 500 ng mL^{-1} with a low detection limit of 0.031 ng mL^{-1} at a *S*/*N* of 3 for AFP determination. The proposed biological recognition and biosensing platform extended the application of ruthenium polypyridyl functionalized ZnO mesocrystals, which provided a new promising prospect.

Introduction

ZnO is regarded as an important wide-band semiconductor material because it has a direct wide band gap of 3.37 eV at room temperature and a large excitation binding energy of 60 meV.[1–3] It has several unique properties including chemical stability,[4] nontoxicity,[5] high specific surface area,[6] high photocatalytic efficiency[7] and strong adsorption ability[8,9] for its versatile applications. Mesocrystals are colloidal crystals with a defined morphology that are built up from nanometer-sized (anisotropic) primary particles.[10] After mesocrystals were first proposed as a new class of ordered nanoparticle superstructures by Cölfen and Antonietti in 2005,[11] ZnO mesocrystals have attracted increasing attention.[12,13] Liu *et al.* reported a low-temperature, polymer-mediated, and one-pot hydrothermal synthesis of unique core–shell structured ZnO mesocrystal microspheres.[14] Considering their high surface area and surface selection, ZnO mesocrystals would arouse scientists' great interest in biological recognition and biosensing.

Graphene has emerged as a fascinating nanomaterial due to its excellent properties such as strong mechanical strength, excellent electronic transport properties and high surface area.[15] The homogeneous aqueous suspensions of graphene were prepared by chemical reduction of graphene oxide (GO) in the presence of chitosan using L-ascorbic acid (L-AA) as a reductant.[16] They have advantages of nontoxic properties, good dispersion and excellent biocompatibility.[16] Gold nanoparticles (AuNPs) have been extensively applied in the detection of aptamers[17] and proteins[18] because of their unique physical and chemical properties. Mao *et al.* reported a biosensor prepared using thermally reduced graphene oxide (TrGO) sheets decorated with AuNP–antibody conjugates.[19] This biosensor avoided nonspecific protein immobilization on TrGO and provided a stable binding for probe proteins through robust AuNPs.[19]

Tris(2,2′-bipyridyl)ruthenium(II) ($Ru(bpy)_3^{2+}$) and its derivatives have received considerable attention due to their good stability and high electrochemiluminescence (ECL) efficiency in aqueous media, favorable electrochemical properties and good compatibility with a wide range of analytes.[20–22] Many efforts have been made using ($Ru(bpy)_3^{2+}$) and its derivatives to fabricate biosensors, such as sandwich-type aptasensors,[23,24] DNA hybridization sensors[25,26] and immunosensors.[27,28] The ECL signal of $Ru(bpy)_3^{2+}$ was too weak to achieve a low detection limit for the biosensor, so some nanoparticles could be used to immobilize more $Ru(bpy)_3^{2+}$ for their large specific surface areas as biolabels for signal amplification. Xu *et al.* reported a $Ru(bpy)_3^{2+}$-based ECL sensor modified with graphene for the determination of tripropylamine (TPrA) and oxalate and good stability was obtained.[29] The introduction of conductive

Jiangsu Key Laboratory of Biofunctional Materials, College of Chemistry and Materials Science, Nanjing Normal University, Nanjing 210023, P. R. China. E-mail: daizhihuii@njnu.edu.cn; Fax: +86-25-85891051; Tel: +86-25-85891051

† These authors contributed equally to this work.

graphene not only facilitated the electron transfer of $Ru(bpy)_3^{2+}$, but also improved the long-term stability of the sensor. But the ECL signal of $Ru(bpy)_3^{2+}$ was still low. Therefore, it is necessary to develop new materials and immobilization methods to improve the intensity further.

In this work, a universal biological recognition and biosensing platform was proposed with a dual signal amplification strategy through ruthenium polypyridyl functionalized ZnO mesocrystals and AuNP dotted reduced graphene oxide (rGO) composite (Scheme 1). The as-synthesized ZnO mesocrystals were served as carriers to load more *N*-succinimidyl ester-bis(hexafluorophosphate) (Ru–NHS ester) and signal antibodies (Ab_2). The AuNP dotted rGO composite modified gold electrode was employed to increase the loading amounts of capture antibodies (Ab_1) and accelerate electron transfer between the detection probe and the electrode. Using AFP as a model, a simple and sensitive sandwich-type electrochemiluminescence biosensor with TPrA as a coreactant for detection of AFP was constructed. The designed biosensor exhibited good performance. The proposed biological recognition and biosensing platform extended the application of ruthenium polypyridyl functionalized ZnO mesocrystals, and showed great potential in clinical diagnosis and detection of low-abundant proteins.

Experimental section

Chemicals and materials

Monoclonal capture and signal AFP antibodies (clone no. 274-1 and 179-2) were purchased from Boson Biotechnology Co. Ltd. (Xiamen, China). AFP, carbohydrate antigen 125 (CA125), and carbohydrateantigen 19-9 (CA19-9) were purchased from Keybio Biotech Co. Ltd. (Beijing, China). Bovine serum albumin (BSA) was purchased from Sigma-Aldrich Chemicals Co. and used without further purification. 1-Ethyl-3-(3-dimethylaminopropyl) carbodiimide (EDC), *N*-hydroxysuccinimide (NHS), chitosan (CS), bis(2,2′-bipyridine)-4′-methyl-4-carboxybipyridine-ruthenium *N*-succinimidyl ester-bis(hexafluorophosphate) (Ru–NHS ester) and tripropylamine (TPrA) were purchased from Sigma-Aldrich Chemicals Co. (St. Louis, MO, USA). Graphene oxide (GO) was purchased from XFNANO Materials Tech Co. Ltd. (Nanjing, China). L-Ascorbic acid (L-AA) powder was purchased from Shanghai Reagent Co. Ltd. (Shanghai, China). All other chemicals were of analytical grade. Phosphate buffered saline (PBS) was prepared by mixing KH_2PO_4 and K_2HPO_4 solutions. Double-distilled water was used throughout the study.

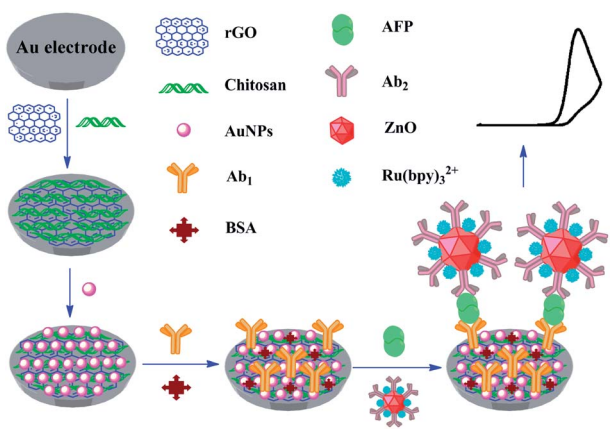

Scheme 1 Schematic diagram of the biological recognition and biosensing platform.

Apparatus

The ECL emission was detected with a model MPI-A electrochemiluminescence analyzer (Xi'An Remax Electronic Science & Technology Co. Ltd., Xi'An, China). All experiments were carried out at room temperature using a conventional three-electrode system with a modified gold electrode (2 mm diameter) as the working electrode, a platinum wire as the auxiliary electrode and an Ag/AgCl electrode as the reference electrode. Ultraviolet-visible (UV-vis) absorption spectra were obtained on a spectrophotometer with 1 cm optical length quartz cell (Cary 50, USA). The X-ray diffraction (XRD) patterns were detected on a powder sample using a D/max-RA X-ray diffractometer (Japan) equipped with graphite monochromatized Cu Kα radiation ($\lambda = 1.54056$ Å) in 2θ ranging from 5° to 85° with a scan rate of 1.2° min^{-1} at 40 kV and 100 mA, respectively. Transmission electrochemical microscopy (TEM) images were taken using a Hitachi H-7650 type transmission electron microscope at an accelerating voltage of 80 kV (Hitachi, Japan). The X-ray energy dispersive spectra (EDS) were recorded on a JSM-5610LV-Vantage typed energy spectrometer. Electrochemical impedance spectroscopy (EIS) was carried out on an Autolab potentiostat/galvanostat PGSTAT302N (Metrohm, Netherland) and controlled by Nova 1.8 software under open-circuit conditions in 0.1 M KCl solution containing 5 mM $K_3Fe(CN)_6/K_4Fe(CN)_6$ (1 : 1). The voltage frequencies ranged from 0.1 Hz to 100 kHz.

Preparation of reduced graphene oxide–chitosan (rGO–CS) suspensions

The rGO–CS suspensions were prepared according to the previous report.[16,30] The GO suspension (100 mL, 0.1 mg mL^{-1}) was gradually added to an acidic aqueous solution of CS (100 mL, 0.5 wt% in 1 wt% acetic acid) with stirring to yield a uniform brown dispersion. L-AA powder (100 mg) was subsequently added to the above dispersion. Then the mixture was held for 6 h at 60 °C for reducing the GO to form the rGO.

Preparation of gold nanoparticles (AuNPs)

The AuNPs were synthesized according to the literature procedure.[31] That is, 100 mL of 1 mM $HAuCl_4$ (4 mL of 1 wt% $HAuCl_4$ solution dissolved in 96 mL of H_2O) was brought to a reflux while stirring and then 10 mL of a 38.8 mM trisodium citrate (10 mL of 1.14 wt% trisodium citrate) solution was added quickly, which resulted in a color change of the solution from pale yellow to deep red. Boiling was continued for 15 min and kept stirring until the sample had cooled to room temperature. The AuNPs were stored at 4 °C until use.

Preparation of ZnO mesocrystals

In a typical synthesis, a solid sample of $Zn(NO_3)_2 \cdot 6H_2O$ (3 mmol), 1-octadecene (8 mL) and dodecylamine (6 mL) were added to a 250 mL three-neck flask at room temperature. Subsequently, the reactor was heated to 280 °C at a rate of 7 °C min^{-1} and kept at that temperature for 30 minutes. Finally, the reactor was naturally cooled down to 50 °C. The crude product was separated and re-dispersed in heptane. Adding absolute ethanol (10 mL) into the dispersed solution, a large quantity of precipitates was produced, which was separated by centrifugation and washed with heptane and absolute ethanol 2–3 times to remove the by-products. Finally, the precipitate was dried in a vacuum for 4 h and used for further characterization and analysis. The yield of ZnO mesocrystals was about 95%.

A mixture of as-prepared ZnO mesocrystals (1 mmol), cyclohexane (15 mL), ethanol (15 mL), and L-lysine (0.1053 g) was stirred at room temperature for 48 h. The product was then isolated by centrifugation with a centrifugal force of 7000 for 10 min, washed with double-distilled water and ethanol. Finally, the precipitate was dried in a vacuum for 4 h and used for further characterization and analysis.[32]

Preparation of Ab_2–ZnO–Ru bioconjugate

The ZnO mesocrystals (5 mg) were dispersed into 10 mL of 1 : 2 ethanol–H_2O by sonicating for 2 h. 1 mg of Ru–NHS ester was predissolved in 200 μL dimethyl sulfoxide (DMSO). 100 μL of 5 mg mL^{-1} Ru–NHS ester and 200 μL of 0.1 mg mL^{-1} Ab_2 were added to 100 μL of 0.5 mg mL^{-1} ZnO suspension. After incubation for 3 h at room temperature in the dark, the mixture was centrifuged at 3000 rpm for 15 min at 4 °C to remove the excess of Ru–NHS ester and Ab_2. After discarding the supernatant, the obtained Ab_2–ZnO–Ru bioconjugate was redispersed in 100 μL of pH 7.4 PBS solution containing 1% BSA, and then stored at 4 °C.

Preparation of the biosensor

The gold electrodes were polished carefully with 0.05 μm α-Al_2O_3 powders on chamois leathers and washed ultrasonically with water and ethanol, respectively. Then the electrodes were electrochemically cleaned in 0.5 M H_2SO_4 with scanning from 0.2 and 1.6 V, followed by drying under nitrogen. 3 μL of rGO–CS suspensions were dropped on the electrode. After the electrode was dried at room temperature for 3 h, it was dipped in the AuNP solution for 8 h. Then the electrode was washed with double-distilled water and immersed into the capture AFP antibody (Ab_1) solution (0.1 mg mL^{-1}) at 4 °C for 12 h. Thereafter, it was rinsed with PBS and incubated in BSA solution (20 μL, 1%) at 37 °C for 1 h to eliminate the nonspecific binding effect. After washing four times with PBS, the electrode was incubated with various concentrations of AFP at 37 °C. After the biological recognition reaction between Ab_1 and AFP, the biosensors were immersed into Ab_2–ZnO–Ru for 50 min at 37 °C followed by washing four times with PBS to remove nonspecifically bound bioconjugates.

Detection conditions

The ECL measurements were performed under scanning from 0.2 to 1.3 V at 100 mV s^{-1} in 0.1 M PBS (pH 7.4) containing 0.5 mM TPrA with a photomultiplier tube voltage of 800 V. Using the proposed biosensor, the ECL responses to different concentrations of AFP were recorded. This system did not need deaeration by nitrogen stripping.

Results and discussion

Characterization of rGO and AuNPs

The formation of rGO from the reduction of GO was investigated by UV-vis spectroscopy (Fig. 1A). As shown in curve a, there were two UV-vis absorption peaks centered at 230 and 300 nm. After the reduction reaction, the maximum absorption bathochromic-shifted from 230 to 270 nm, and meanwhile the absorption peak at 300 nm disappeared (curve b), suggesting that rGO was formed from the reduction of GO and its aromatic structure was retained. From the XRD image in Fig. 1C, within the $5° < 2\theta < 50°$ range, only one obvious and sharp diffraction peak could be observed, indicating that GO was crystalline. After the reduction reaction, the sharp diffraction peak disappeared, confirming that rGO was formed.

The UV-vis absorption spectrum displayed the absorption spectra of the AuNPs with the maximum plasmon absorption peak at *ca.* 520 nm, which was a characteristic absorption of AuNPs (Fig. 1B), indicating the successful synthesis of AuNPs. The formed AuNPs were further characterized using the TEM image (Fig. 2). AuNPs were well dispersed and the average size was about 12.3 nm (the inset in Fig. 2), which was suitable for immobilizing proteins.

Characterization of ZnO mesocrystals

Fig. 3 shows the XRD pattern of ZnO mesocrystals. The characteristic diffraction peaks of the sample fitted well with the

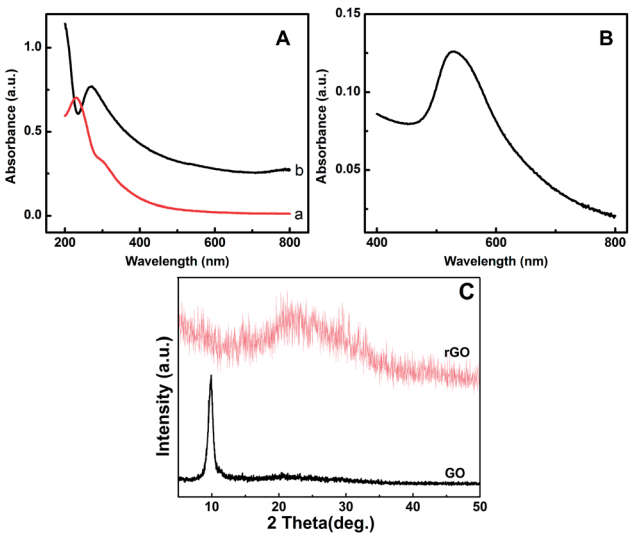

Fig. 1 UV-vis spectra of (A) GO aqueous dispersions before (a) and after (b) being reduced by L-AA for 6 hours; (B) AuNPs; and (C) XRD patterns of GO and rGO.

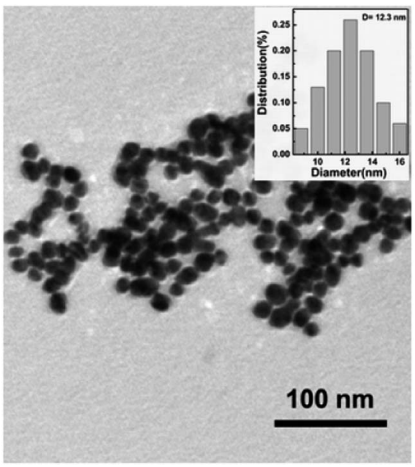

Fig. 2 TEM image of AuNPs (inset: the statistical size of the AuNPs).

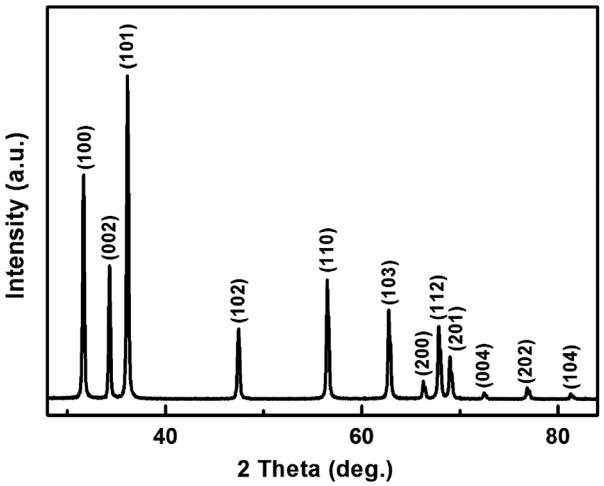

Fig. 3 The XRD pattern of ZnO mesocrystals.

hexagonal phase ZnO crystal structure (the ASTM standard 80-75). No other crystalline impurities and no remarkable shift of all diffraction peaks were detected. TEM (Fig. 4A) and SEM (Fig. 4B) images show unique well-faceted ZnO mesocrystals which were beneficial for loading more Ru–NHS ester and signal antibodies.

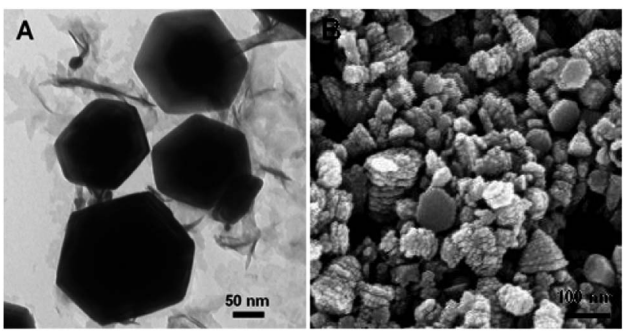

Fig. 4 The TEM (A) and SEM (B) images of ZnO mesocrystals.

Characterization of the Ab_2–ZnO–Ru bioconjugate

The EDS patterns of ZnO mesocrystals and Ab_2–ZnO–Ru bioconjugate are shown in Fig. 5. The EDS pattern of ZnO mesocrystals shows only the presence of Zn and O elements (Fig. 5A). After the Ru–NHS ester and the Ab_2 molecules were attached to the surface of ZnO mesocrystals, the Ru element was observed on the EDS pattern of the Ab_2–ZnO–Ru bioconjugate (Fig. 5B), indicating the Ru–NHS ester immobilized on the surface of ZnO mesocrystals. Besides, the C element was found to be present and the intensity of the O element was increased, which suggested that the Ab_2 had been immobilized on the surface of ZnO mesocrystals. The P and K elements were also observed, which might come from PBS.

Characterization of the biosensor

Electrochemical impedance spectroscopy (EIS) is an effective tool for investigating the modification process of the biosensing interface. Therefore, it was carried out to characterize the fabrication process of the proposed biosensor. The EIS spectra were obtained in 0.1 M KCl solution containing 5.0 mM $[Fe(CN)_6]^{4-}/[Fe(CN)_6]^{3-}$. As seen in the EIS spectra (Fig. 6), the bare gold electrode revealed a small resistance (curve a). After the suspensions of rGO–CS were modified on the gold electrode, a lower resistance was observed (curve b). The reason may be that the formed rGO–CS membrane accelerated the interfacial

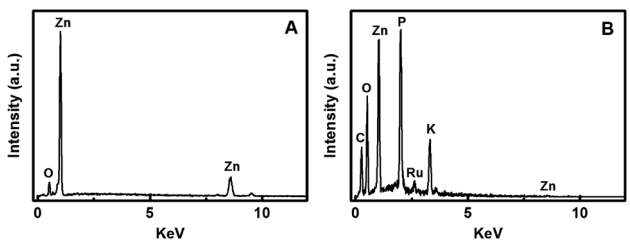

Fig. 5 The EDS patterns of ZnO mesocrystals (A) and Ab_2–ZnO–Ru bioconjugate (B).

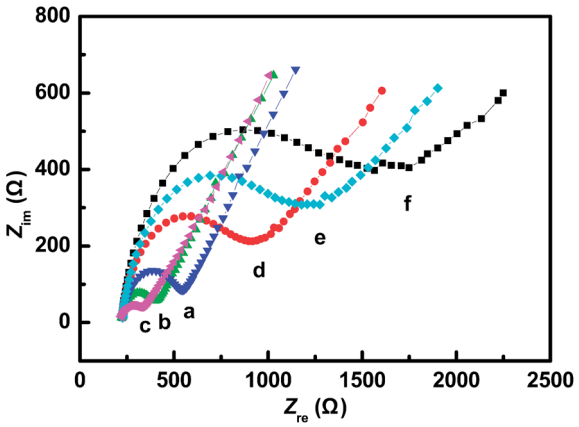

Fig. 6 Electrochemical impedance spectra of different electrodes: (a) bare Au, (b) Au/rGO–CS, (c) Au/rGO–CS/AuNPs, (d) Au/rGO–CS/AuNP/Ab_1, (e) Au/rGO–CS/AuNP/Ab_1/AFP and (f) Au/rGO–CS/AuNP/Ab_1/AFP/Ab_2–ZnO–Ru in 0.1 M KCl aqueous solution containing 5.0 mM $[Fe(CN)_6]^{3-/4-}$ (1 : 1).

electron transfer between the $[Fe(CN)_6]^{3-/4-}$ redox probe and the electrode surface. The electron-transfer resistance (R_{et}) was the lowest at the rGO–CS/AuNP-modified electrode (curve c) due to the excellent electronic conductivity of AuNPs. After the electrode was modified with Ab_1, an increase of R_{et} was observed (curve d) owing to the fact that Ab_1 hindered the movement of the $[Fe(CN)_6]^{3-/4-}$ redox probe towards the electrode surface. The stepwise assembly of AFP and Ab_2–ZnO–Ru on the electrode surface was accompanied by an increase of R_{et} (curves e and f). Similarly, both AFP and Ab_2–ZnO–Ru could resist the electron-transfer kinetics of the redox probe at the electrode interface, resulting in the increasing impedance of the electrode, which confirmed the successful preparation of the biosensor.

ECL response of the biosensor

As shown in Fig. 7, compared with the Au/Ab_1/AFP/Ab_2–Ru (curve a), Au/rGO–CS/AuNP/Ab_1/AFP/Ab_2–Ru exhibited a small increase in ECL intensity (curve b), indicating that rGO and AuNPs could accelerate electron transfer between the detection probe and the electrode together with improving the absorption capacity of the antibody. However, using Ru–NHS ester-functionalized ZnO mesocrystals as bionanolabels, the biosensor (curve c) exhibited a remarkably higher ECL response than Ru–NHS ester labeled Ab_2 (curve b). ZnO mesocrystals displayed a high specific surface area, which could enhance the immobilized amount of proteins. The ZnO mesocrystals as carriers loaded more Ru–NHS esters and antibodies to amplify the ECL signal output, leading to a much improved ECL response of the proposed biosensor. Therefore, a universal biological recognition and biosensing platform was designed with a dual signal amplification strategy from Ru–NHS ester functionalized ZnO mesocrystals and AuNP dotted rGO composite (Scheme 1).

Effects of the detection solution pH and incubation time on the responses of the biosensor

The pH of the detection solution was important for the activity of the protein and the ECL reaction of TPrA with $Ru(bpy)_3^{2+}$,[33] thus the effect of pH from 5.0 to 9.0 on the biosensor performance was investigated in this work. As shown in Fig. 8A, the maximum ECL response appeared at pH 7.4. Therefore, 7.4 was chosen as the pH value of the detection solution.

The incubation time greatly affected the analytical performance of the proposed biosensor.[34] It can be seen that the ECL response enhanced with increasing incubation time and then tended to a plateau after 50 min (Fig. 8B). Thus, 50 min was selected as the optimal incubation time.

Biosensing for AFP

Under the optimal conditions, the ECL response of the biosensor increased with the increment of AFP concentrations and exhibited a good linear relationship with the logarithm of the AFP concentration from 0.04 to 500 ng mL^{-1} (Fig. 9). The linear equation was $I = 1808.47 + 1165.88 \log(C_{AFP})$ with a correlation coefficient of 0.9962 and a detection limit of 0.031 ng mL^{-1} at a S/N of 3. The detection limit of 0.031 ng mL^{-1} was much lower than 2.06 ng mL^{-1} by the colorimetric method and 12.5 ng mL^{-1} by the microfluidic technique.[35,36] The linear response range of 0.04 to 500 ng mL^{-1} was wider than those of 0.25 to 100 ng mL^{-1} by the electrochemical method and 1 to 80 ng mL^{-1} by the chemiluminescence method.[37,38] In addition,

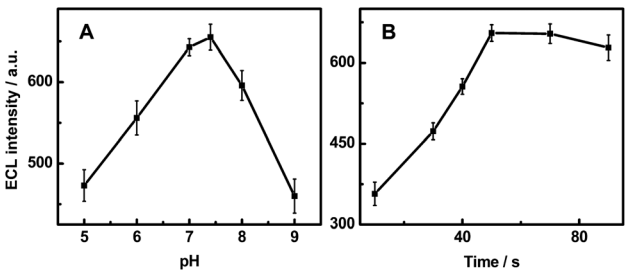

Fig. 8 Effects of (A) the detection solution pH and (B) incubation time on the responses of the ECL biosensor towards 0.1 ng mL^{-1} AFP.

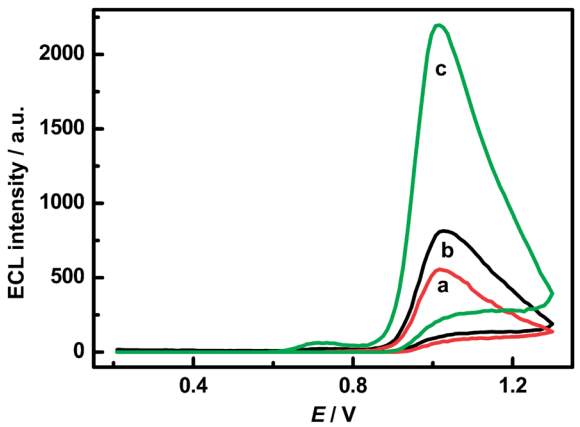

Fig. 7 ECL responses of (a) Au/Ab_1/AFP/Ab_2–Ru, (b) Au/rGO–CS/AuNP/Ab_1/AFP/Ab_2–Ru and (c) Au/rGO–CS/AuNP/Ab_1/AFP/Ab_2–ZnO–Ru in 0.1 M PBS (pH 7.4) containing 0.5 mM TPrA. The AFP concentration was 2.1 ng mL^{-1}.

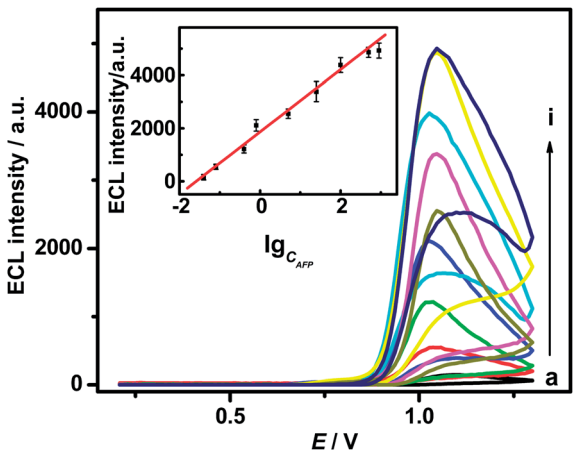

Fig. 9 ECL responses of the proposed biosensor to different concentrations of AFP (ng mL^{-1}): (a) 0.04, (b) 0.08, (c) 0.4, (d) 0.8, (e) 5, (f) 25, (g) 100, (h) 500, and (i) 600. Inset: a linear plot for AFP determination.

the detection peak potential was recorded for ECL assay at +1.01 V, which was more negative than +1.35 V by using the ECL sensor made with $Ru(bpy)_3^{2+}$ derivatives[39] and +1.13 V using the ECL sensor made with $Ru(bpy)_3^{2+}$-doped silica nanoparticles,[40] leading to less interference. Thus the biosensor showed a wide linear response range and high sensitivity in the determination of AFP.

To evaluate the specificity of the biosensor, the effects of some proteins (BSA, CA125 and CA19-9) as interfering species on the ECL response of the biosensor were examined (Fig. 10A). Compared with the ECL response of the biosensor towards 0.3 ng mL^{-1} AFP (curve a), the proposed biosensor did not show any significant responses towards 400 ng mL^{-1} BSA (curve b), 0.3 ng mL^{-1} CA125 (curve c) and 0.3 ng mL^{-1} CA19-9 (curve d), respectively, suggesting that the above proteins interfered less in the AFP detection. Therefore, the as-prepared biosensor would have acceptable selectivity for monitoring of AFP in clinical serum samples.

The reproducibility of the proposed biosensor was assessed by the relative standard derivations (RSDs) of intra-assay and inter-assay. The RSDs of intra-assay and inter-assay were 4.5% and 4.8%, respectively, for six measurements at the AFP concentration of 0.1 ng mL^{-1}. Thus the proposed biosensor exhibited acceptable reproducibility. Moreover, no obvious changes of the ECL intensities (1.1% variation) were observed after the biosensor scanned by consecutive cyclic voltammograms (CVs) for 8 cycles (Fig. 10B), indicating good stability for ECL detection.

The analysis of AFP in the serum samples was carried out without any need for sample pretreatment. The accuracy using the designed biosensor for ECL determination of AFP was examined by comparing the results obtained through our strategy with the commercial turbidimetric immunoassay provided by the Jiangsu Institute of Cancer Prevention and Cure. The assay results of clinical serum samples, compared with the reference values obtained by commercial turbidimetric immunoassay, showed acceptable agreement with relative errors less than 10.2% (Table 1), suggesting acceptable accuracy.

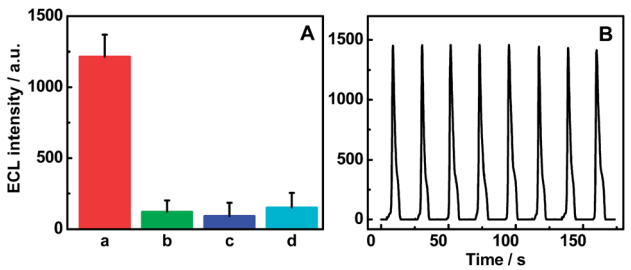

Fig. 10 (A) ECL response of the proposed biosensor towards: (a) 0.3 ng mL^{-1} AFP, (b) 400 ng mL^{-1} BSA, (c) 0.3 ng mL^{-1} CA125 and (d) 0.3 ng mL^{-1} CA19-9 in 0.1 M PBS (pH 7.4) containing 0.5 mM TPrA; (B) ECL response of the proposed biosensor towards 0.5 ng mL^{-1} AFP under continuous CVs for 8 cycles.

Table 1 Assay results of clinical serum samples using the proposed and reference methods

Analyte	AFP (ng mL^{-1})		
Sample no.	1	2	3
Proposed method	4.07	8.72	45.80
Reference method	3.85	9.66	41.56
Relative error (%)	5.7	−9.7	10.2

Conclusions

A universal biological recognition and biosensing platform was developed with a dual signal amplification strategy using Ru–NHS ester functionalized ZnO mesocrystals and AuNP dotted rGO composite. The ZnO mesocrystals as carriers loaded more Ru–NHS ester and signal antibodies to amplify the ECL signal output. rGO and AuNPs could accelerate electron transfer between the detection probe and the electrode together with improving the absorption capacity of capture antibodies. The synergic effect of ZnO mesocrystals and AuNP dotted rGO composite significantly improved the ECL response, leading to a good performance of the proposed biosensors. Using AFP as a model, a simple and sensitive sandwich-type electrochemiluminescence biosensor for detection of AFP was proposed. The designed biosensor could be successfully applied to the analysis of clinical samples and exhibited good performance such as a wide linear response range, high sensitivity and good stability. Using Ru–NHS ester functionalized ZnO mesocrystals and AuNP dotted rGO composite for developing a biological recognition and biosensing platform extended their applications, which provides a promising prospect in clinical diagnosis and protein monitoring.

Acknowledgements

This work was supported by the NSFC (21175069, 21171096 and 21205061), Research Fund for the Doctoral Program of Higher Education of China (20113207110005) and Foundation of the Jiangsu Education Committee (11KJA150003). We appreciate the financial support from the PAPD of Jiangsu Higher Education Institutions and the Program for Jiangsu Collaborative Innovation Center of Biomedical Functional Materials.

Notes and references

1 S. Bai, W. W. Wu, Y. Qin, N. Y. Cui, D. J. Bayerl and X. D. Wang, *Adv. Funct. Mater.*, 2011, **21**, 4464–4469.
2 X. Jin, M. Gotz, S. Wille, Y. K. Mishra, R. Adelung and C. Zollfrank, *Adv. Mater.*, 2013, **25**, 1342–1347.
3 S. M. Hatch, J. Briscoe and S. Dunn, *Adv. Mater.*, 2013, **25**, 867–871.
4 M. H. Huang, S. Mao, H. Feick, H. Q. Yan, Y. Y. Wu, H. Kind, E. Weber, R. Russo and P. D. Yang, *Science*, 2001, **292**, 1897–1899.
5 A. Kim, Y. Won, K. Woo, C. H. Kim and J. Moon, *ACS Nano*, 2013, **7**, 1081–1091.
6 Z. W. Pan, Z. R. Dai and Z. L. Wang, *Science*, 2001, **291**, 1947–1949.

7 C. Y. Wen, F. Liao, S. S. Liu, Y. Zhao, Z. H. Kang, X. L. Zhang and M. W. Shao, *Chem. Commun.*, 2013, **49**, 3049–3051.
8 T. D. Zaveri, N. V. Dolgova, B. H. Chu, J. Lee, J. Wong, T. P. Lele, F. Ren and B. G. Keselowsky, *Biomaterials*, 2010, **31**, 2999–3007.
9 S. Z. Yang, L. F. Wang, X. Z. Tian, Z. Xu, W. L. Wang, X. D. Bai and E. G. Wang, *Adv. Mater.*, 2012, **24**, 4676–4682.
10 Z. H. Li, A. Gesßner, J. P. Richters, J. Kalden, T. Voss, C. Kübel and A. Taubert, *Adv. Mater.*, 2008, **20**, 1279–1285.
11 H. Cölfen and M. Antonietti, *Angew. Chem., Int. Ed.*, 2005, **44**, 5576–5591.
12 M. H. Liu, Y. H. Tseng, H. F. Greer, W. Z. Zhou and C. Y. Mou, *Chem.–Eur. J.*, 2012, **18**, 16104–16113.
13 M. Distaso, R. N. K. Taylor, N. Taccardi, P. Wasserscheid and W. Peukert, *Chem.–Eur. J.*, 2011, **17**, 2923–2930.
14 Z. Liu, X. D. Wen, X. L. Wu, Y. J. Gao, H. T. Chen, J. Zhu and P. K. Chu, *J. Am. Chem. Soc.*, 2009, **131**, 9405–9412.
15 L. Wang, M. Xu, L. Han, M. Zhou, C. Z. Zhu and S. J. Dong, *Anal. Chem.*, 2012, **84**, 7301–7307.
16 M. Fang, J. Long, W. F. Zhao, L. W. Wang and G. H. Chen, *Langmuir*, 2010, **26**, 16771–16774.
17 E. Yasun, B. Gulbakan, I. Ocsoy, Q. Yuan, M. I. Shukoor, C. Li and W. Tan, *Anal. Chem.*, 2012, **84**, 6008–6015.
18 R. Malhotra, V. Patel, B. V. Chikkaveeraiah, B. S. Munge, S. C. Cheong, R. B. Zain, M. T. Abraham, D. K. Dey, J. S. Gutkind and J. F. Rusling, *Anal. Chem.*, 2012, **84**, 6249–6255.
19 S. Mao, G. H. Lu, K. H. Yu, Z. Bo and J. H. Chen, *Adv. Mater.*, 2010, **22**, 3521–3526.
20 M. Shao, L. Yan, H. P. Pan, I. Ivanov and B. Hu, *Adv. Mater.*, 2011, **23**, 2216–2220.
21 R. Kurita, K. Arai, K. Nakamoto, D. Kato and O. Niwa, *Anal. Chem.*, 2010, **82**, 1692–1697.
22 D. M. Benoist and S. L. Pan, *J. Phys. Chem. C*, 2010, **114**, 1815–1821.
23 L. J. Bai, R. Yuan, Y. Q. Chai, Y. Zhuo, Y. L. Yuan and Y. Wang, *Biomaterials*, 2012, **33**, 1090–1096.
24 Y. Li, H. L. Qi, Q. Gao and C. X. Zhang, *Biosens. Bioelectron.*, 2011, **26**, 2733–2736.
25 L. Y. Feng, Y. Chen, J. S. Ren and X. G. Qu, *Biomaterials*, 2011, **32**, 2930–2937.
26 S. W. Bae, J. W. Oh, I. S. Shin, M. S. Cho, Y. R. Kim, H. Kim and J. I. Hong, *Analyst*, 2010, **135**, 603–607.
27 L. Ge, J. X. Yan, X. R. Song, M. Yan, S. G. Ge and J. H. Yu, *Biomaterials*, 2012, **33**, 1024–1031.
28 N. P. Sardesai, J. C. Barron and J. F. Rusling, *Anal. Chem.*, 2011, **83**, 6698–6703.
29 M. S. Wu, H. W. Shi, L. J. He, J. J. Xu and H. Y. Chen, *Anal. Chem.*, 2012, **84**, 4207–4213.
30 H. J. Li, J. Chen, S. Han, W. X. Niu, X. Q. Liu and G. B. Xu, *Talanta*, 2009, **79**, 165–170.
31 J. J. Storhoff, R. Elghanian, R. C. Mucic, C. A. Mirkin and R. L. Letsinger, *J. Am. Chem. Soc.*, 1998, **120**, 1959–1964.
32 Y. Zhang, G. S. Hong, Y. J. Zhang, G. C. Chen, F. Li, H. J. Dai and Q. B. Wang, *ACS Nano*, 2012, **6**, 3695–3702.
33 L. Mao, R. Yuan, Y. Q. Chai, Y. Zhuo, X. Yang and S. R. Yuan, *Talanta*, 2010, **80**, 1692–1697.
34 M. R. Kanda, Y. L. Choe and H. Yang, *Anal. Chem.*, 2012, **84**, 1049–1055.
35 C. A. Mandon, O. I. Berthuy, B. P. Corgier, G. C. Le Goff, P. Faure, L. J. Blum and C. A. Marguette, *Biosens. Bioelectron.*, 2013, **39**, 37–43.
36 C. J. Huang, H. I. Lin, S. C. Shiesh and G. B. Lee, *Biosens. Bioelectron.*, 2012, **35**, 50–55.
37 C. L. Hong, R. Yuan, Y. Q. Chai, Y. Zhuo and X. Yang, *J. Electroanal. Chem.*, 2012, **664**, 20–25.
38 Z. J. Yang, H. Liu, C. Zong, F. Yan and H. X. Ju, *Anal. Chem.*, 2009, **81**, 5484–5489.
39 B. Sun, H. L. Qi, F. Ma, Q. Gao, C. X. Zhang and W. J. Miao, *Anal. Chem.*, 2010, **82**, 5046–5052.
40 W. J. Qi, D. Wu, J. M. Zhao, Z. Y. Liu, W. Zhang, L. Zhang and G. B. Xu, *Anal. Chem.*, 2013, **85**, 3207–3212.